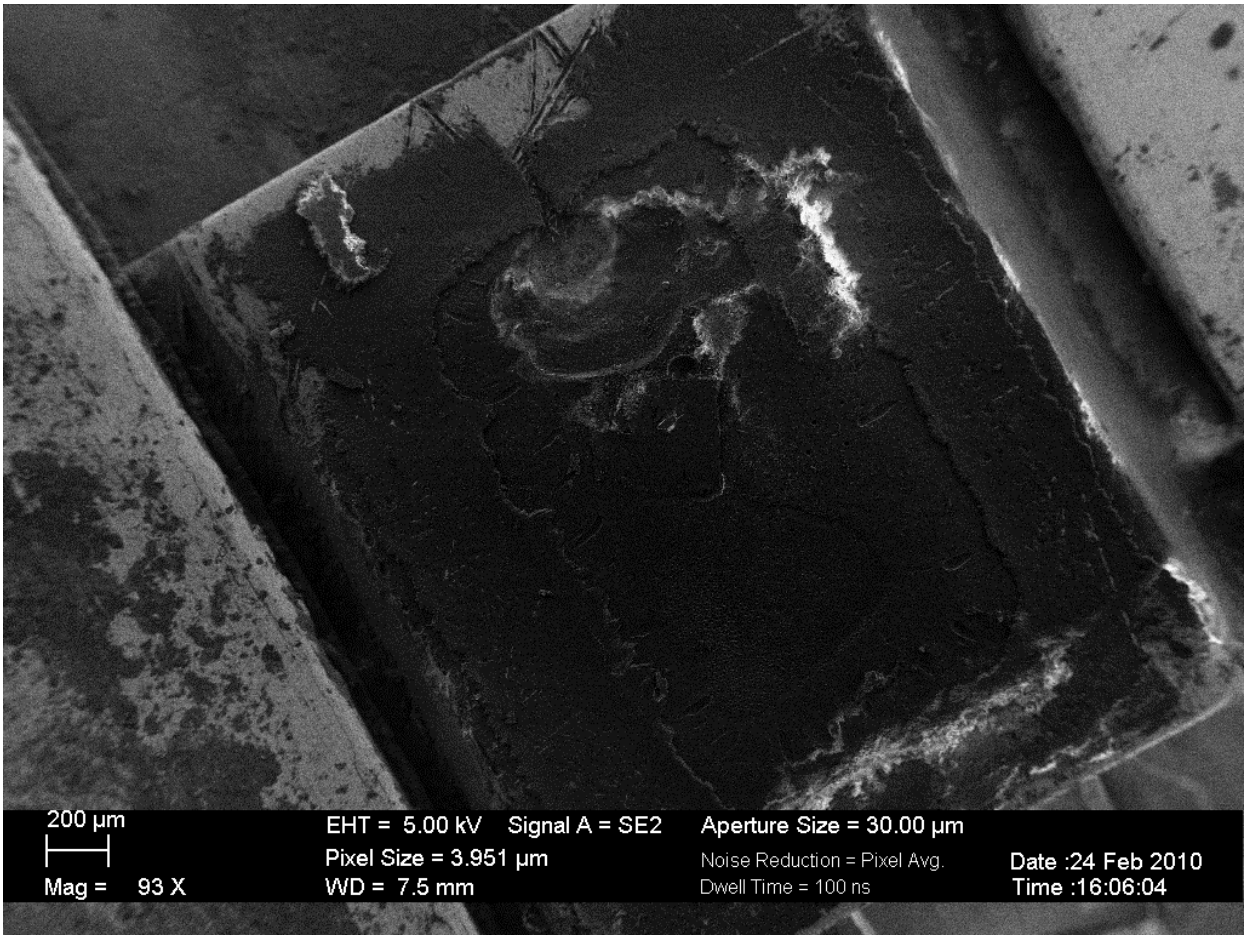

Supplementary Figure S1. Low magnification image showing one half of the "sandwich holder" from the top. The rectangular print left by the water droplet contained in the holder cavity (inner rectangular mark) in the frozen decane (dark background) is clearly visible.

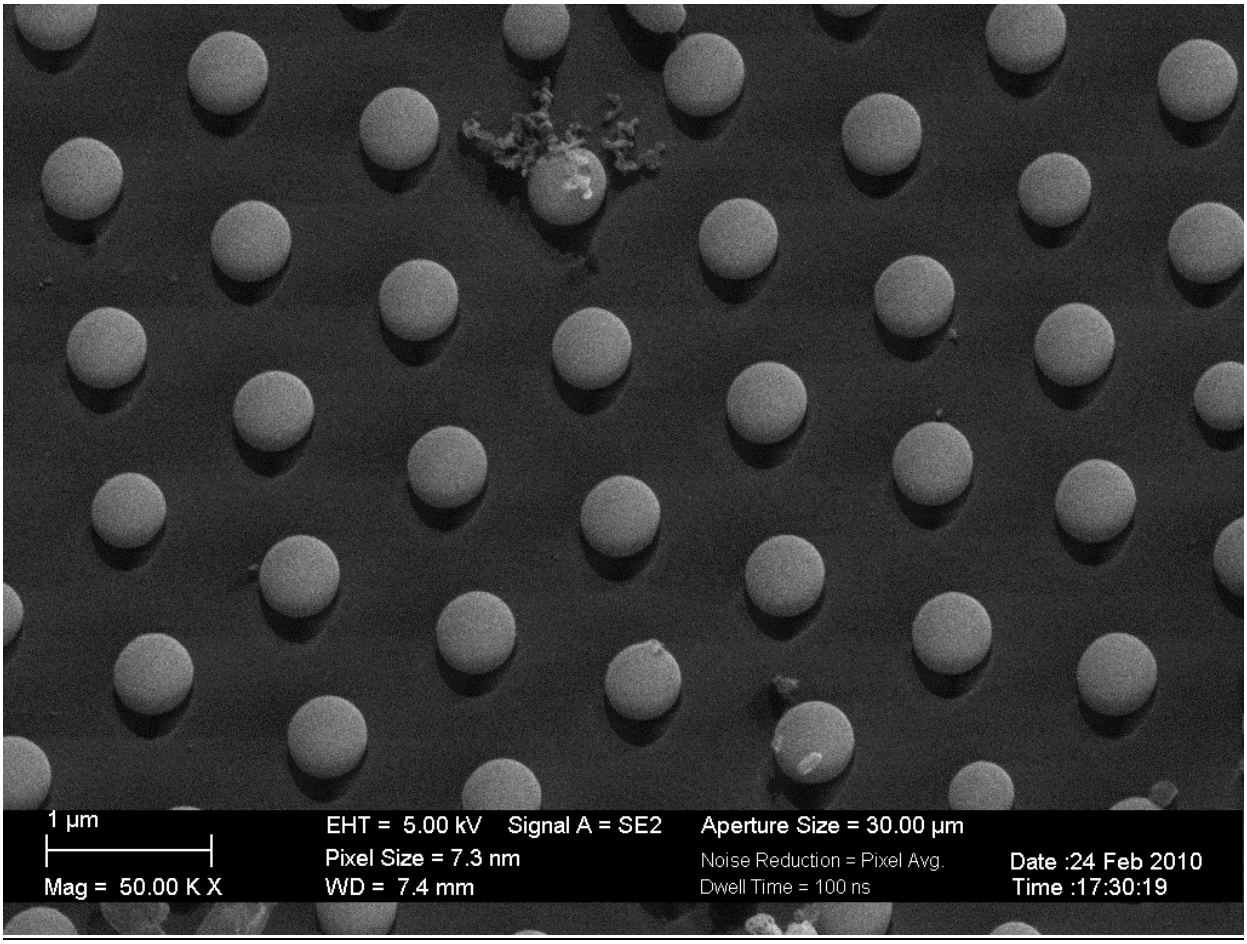

Supplementary Figure S2. Self-assembled monolayer of 500 nm amidine latex nanoparticles at the decane/water interface. The presence of long-range order is clearly visible.

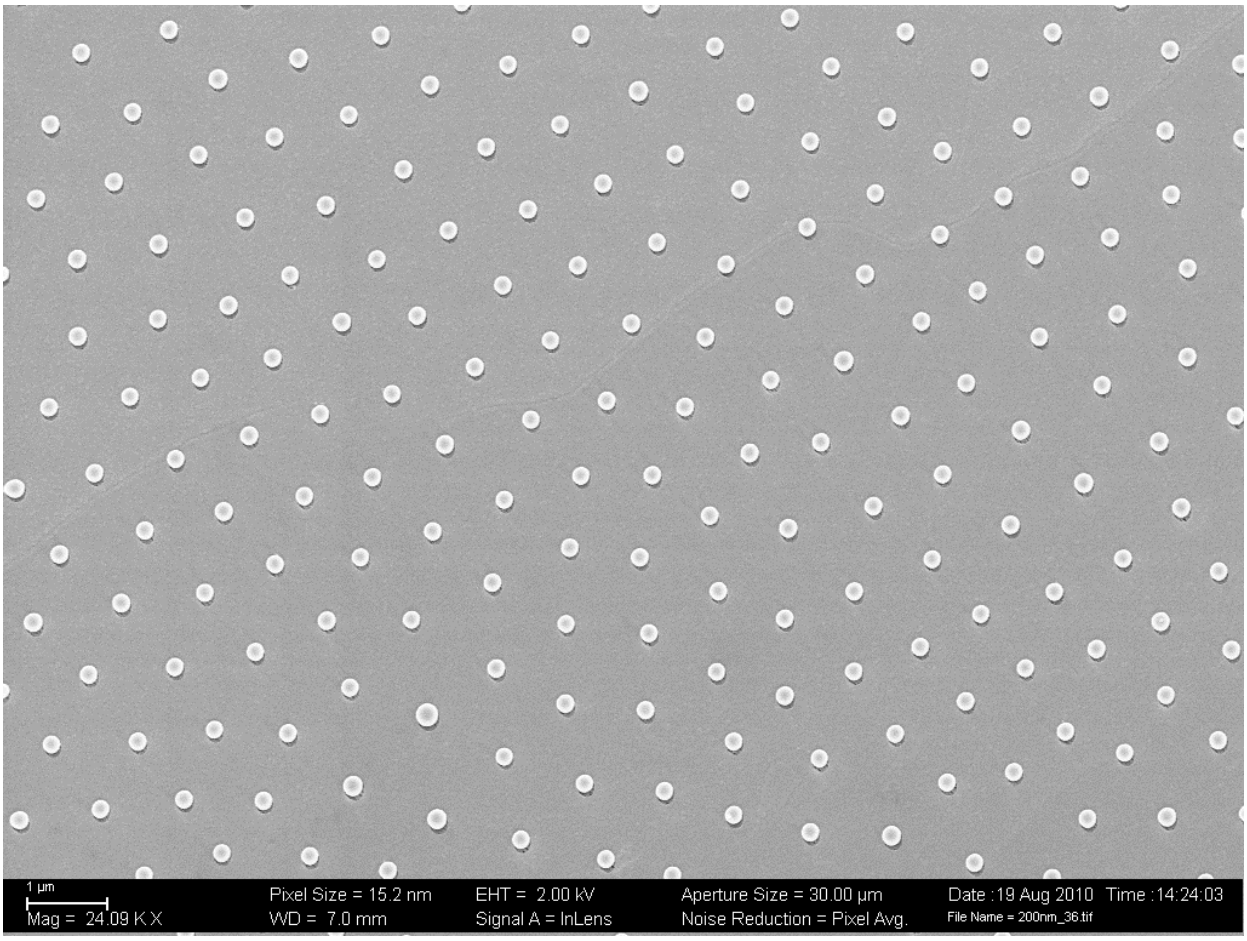

Supplementary Figure S3. Self-assembled monolayer of 200 nm amidine latex nanoparticles at the decane/water interface. The presence of long-range order is clearly visible.

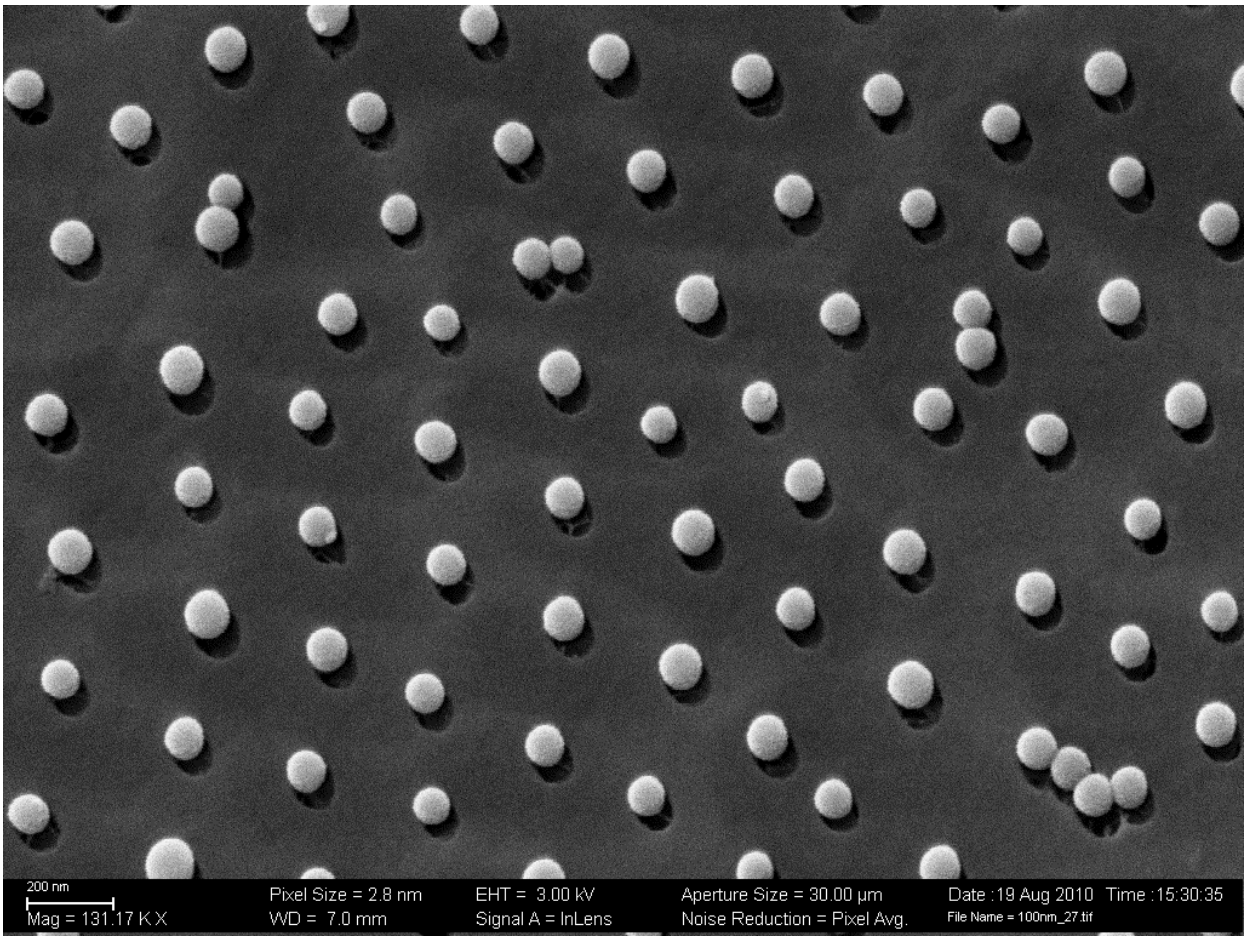

Supplementary Figure S4. Self-assembled monolayer of 100 nm amidine latex nanoparticles at the decane/water interface. The presence of long-range order is clearly visible but, thanks to imaging individual entities, a small number of aggregating particles is directly detectable.

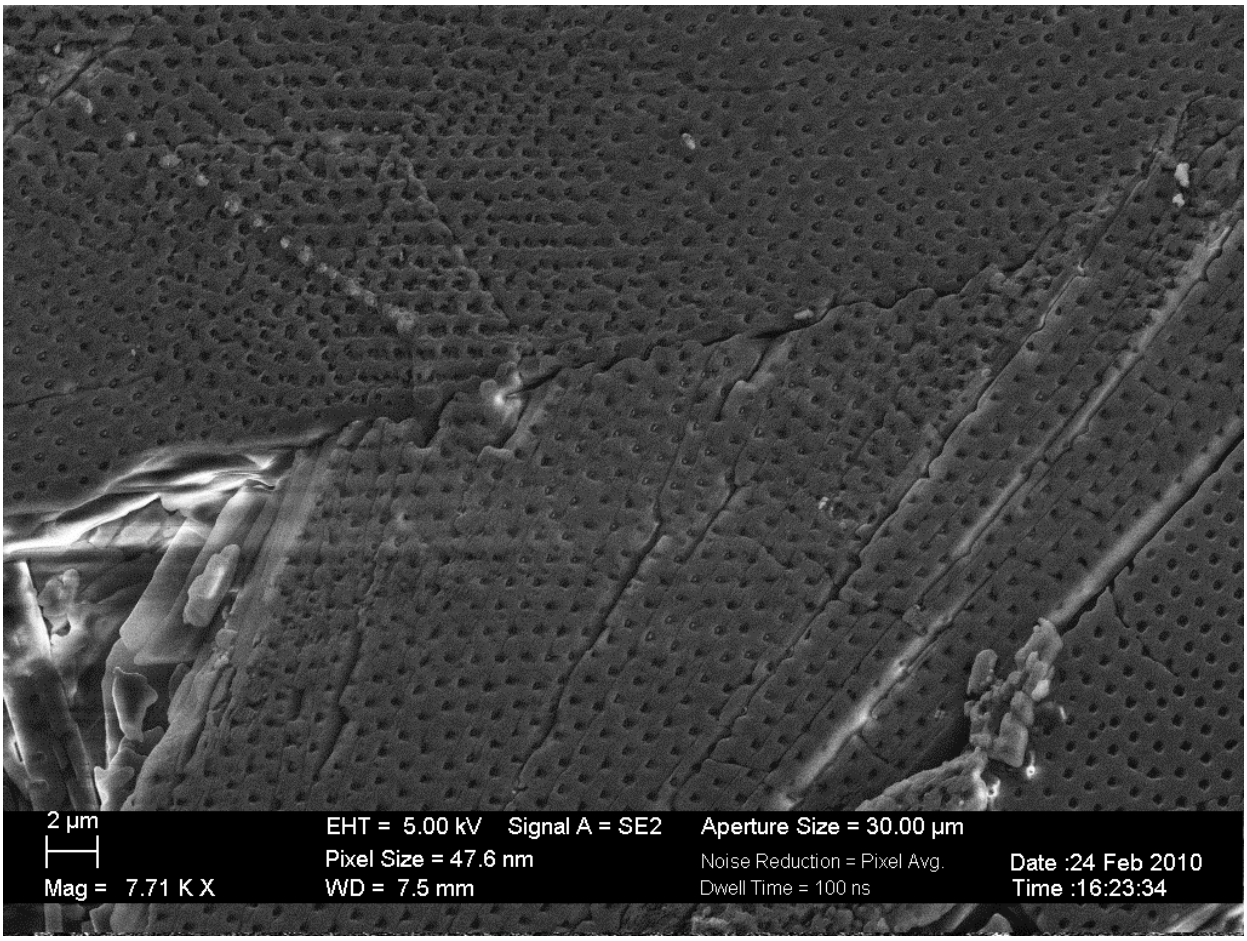

Supplementary Figure S5. Image of long-range ordered arrays of prints left by 500 nm particles in frozen decane. Decane crystals below the interface are visible on the left side of the image.

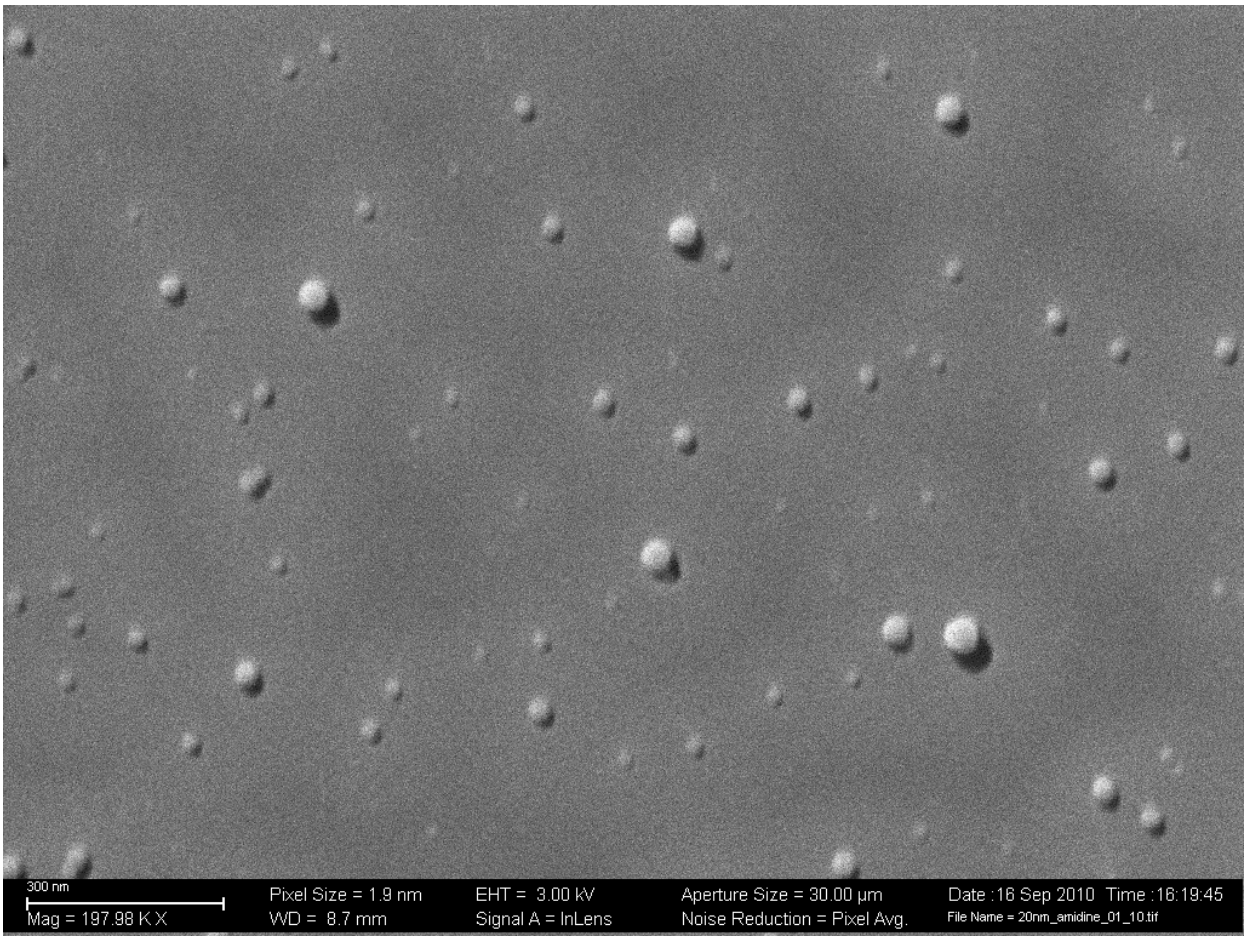

Supplementary Figure S6. Image of 20 nm amidine latex particles at the hexane/water interface. The high particle polydispersity as well as the wide distribution of contact angles can be inferred from the image. For the case of small NPs, locating correctly the interface plane may prove challenging; in order to overcome this obstacle, 500 nm amidine latex particles were added as "seeds" (not shown) to help find the interface, and then higher magnifications were used to image the smaller colloids.

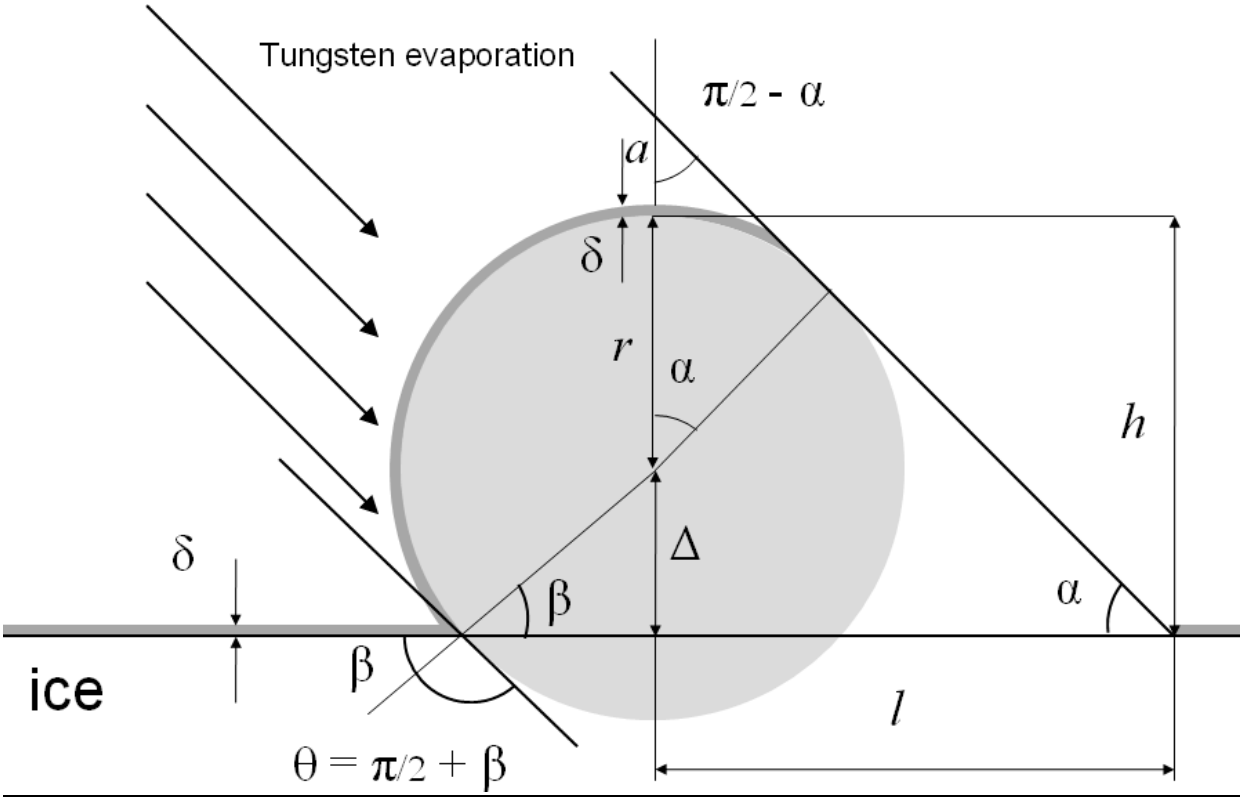

Supplementary Figure S7. Schematic representation of a hydrophobic particle frozen at the interface after tungsten deposition.

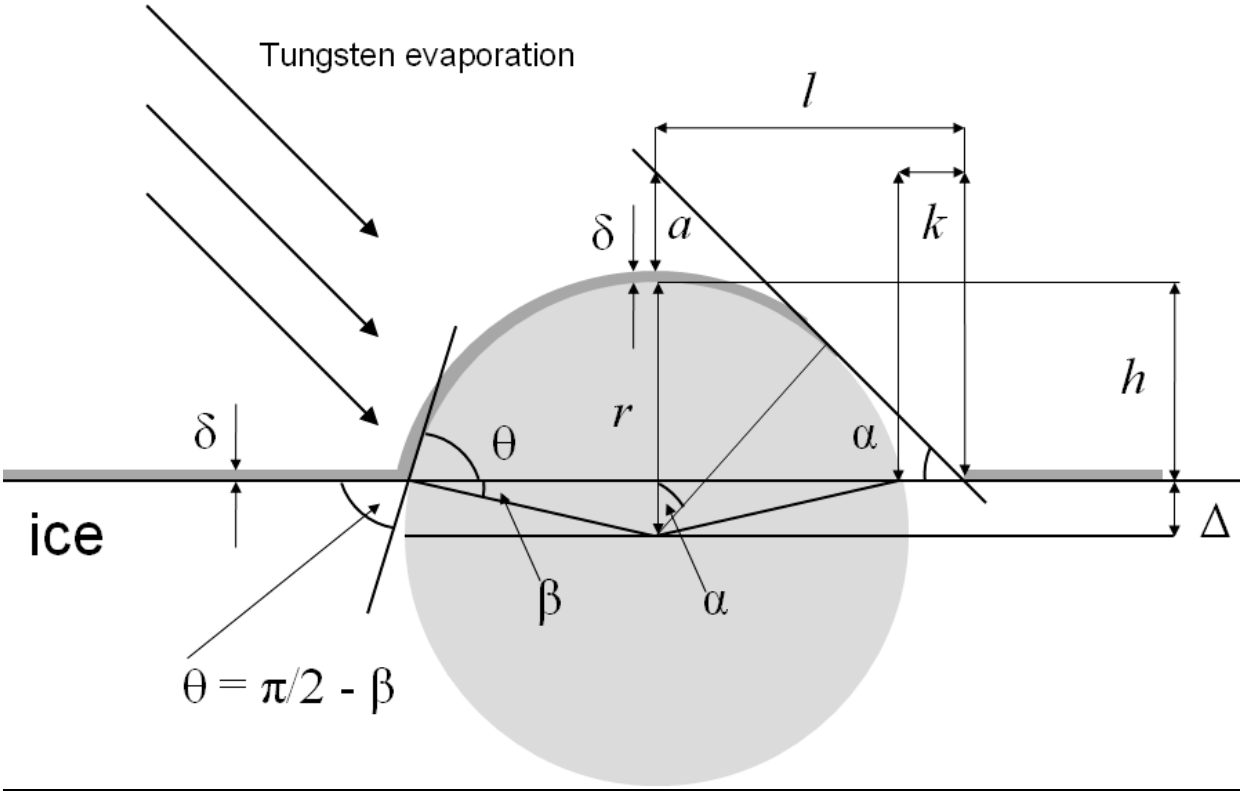

Supplementary Figure S8. Schematic representation of a hydrophilic particle frozen at the interface after tungsten deposition.

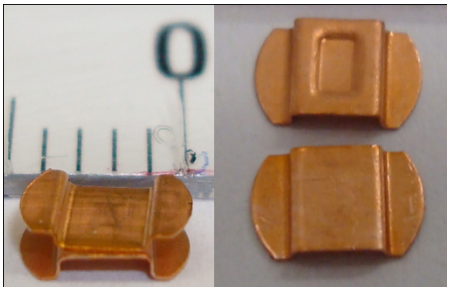

Supplementary Figure S9. Close up of the freeze fracture specimen carrier. Left: closed after sample loading. Right: open. The cavity which holds the suspension is clearly visible in the right image (top).

Supplementary Table S1. Amidine latex polystyrene nanoparticle specifications for the used batches according to the supplier (Invitrogen/IDC)

Particle batch #	Nominal size [nm]	Mean diameter [nm]	CV [%]	Surface charge density as NH_2 [μC/cm²]
2195	500	510±23	4.6	19.7
2231	200	220±10	4.3	13.2
2204	100	90±7	8.3	5.2
2197	40	44±6	12.8	3.4
2195	20	23±5	21.9	3.0

Supplementary Table S2. Citrate gold nanoparticle particle specifications for the used batches according to the supplier (BBI International)

Particle batch #	Nominal size [nm]	Mean diameter range [nm]	CV [%]	Surface charge density
12257	100	96.0-104.0	< 8	n.a.
13147	20	19.0-21.0	< 8	n.a.

Supplementary Table S3. Specifications for additional colloidal particles used in this work

Particle batch #	Nominal size [nm]	Mean diameter [nm]	CV [%]	Surface charge density	Supplier
PPMA-asm270	2200	2174	< 6	n.a.	Dr. A Schofiled (Edinburgh University, UK)
Sulfate Latex 1140,1	100	92	n.a	n.a.	Invitrogen/IDC, UK
Polystyrene PS-Fluo-3.0/Fil35	2800	2800±40	1.6	n.a.	Microparticles GmBH, Germany

Supplementary Note 1

Calculation of the single-particle contact angles

In this section we present a detailed derivation of the single-particle contact angles from the experimental data. Below we define the quantities necessary for the derivation:

r = particle radius

δ = tungsten layer thickness

k = measured length of the shadow

l = measured distance from particle centre to edge of the shadow

h = particle height relative to the interface

Δ = position of the particle centre relative to the interface

a = projected distance along the particle vertical

α = metal deposition angle

θ = particle contact angle

β = angle between interface and particle radius at contact point

Depending on whether the particles are hydrophilic or hydrophobic, different derivations are required.

Hydrophobic particles

From geometrical considerations we can write:

$$(r + a + \delta) = \frac{r}{\cos(\alpha)} \quad \rightarrow \quad a = r\left[\frac{1}{\cos[(\alpha) - 1]} - \delta\right] \qquad \text{(S1)}$$

$$(\Delta + r + \delta + a) = l\,tan(\alpha) \qquad \text{(S2)}$$

substituting (S1) into (S2) we get

$$l - \frac{r}{\sin(\alpha)} \qquad] \qquad \text{(S3)}$$

from Fig. S7 we see that $\theta = {}^{\pi}/_{2} + \beta$, and

$$\beta = \arcsin\left({}^{\Delta}/_{r}\right), \qquad \text{(S4)}$$

so finally the expression for the contact angle is:

$$\theta = {}^{\pi}\Big/_{2 + \sin^{-1}\left[\frac{\tan(\alpha)\left[l - \frac{r}{\sin(\alpha)}\right]}{r}\right]} = {}^{\pi}/_{2} + \sin^{-1}\left[\tan(\alpha)\frac{l}{r} - \frac{1}{\cos(\alpha)}\right] \qquad \text{(S5)}$$

We point out that in the case of hydrophobic particles, since the equatorial diameter of the particle is exposed, both r and l can be measured directly for each particle. Moreover, the measured contact angle depends only on the ratio l/r which is used in the derivation of the method's accuracy below.

In the case of neutrally wetting particles, θ equals π/2 and therefore Δ=0. This gives a very easy criterion to determine the wettability of the particle from eq. (S3) (and thus the formula needed to calculate θ).

For θ=π/2, $l = r/\sin(\alpha)$ and therefore if:

$$l > \frac{r}{\sin(\alpha)} \quad \Rightarrow \quad \textbf{hydrophobic particle}$$

$$l < \frac{r}{\sin(\alpha)} \quad \Rightarrow \quad \textbf{hydrophilic particle}$$

$l = r/\sin(\alpha)$ constitutes the lower limit for l in the case of hydrophobic particles; the upper limit is found by imposing the condition $\max(\theta) = \pi$, which from eq. (S5) yields

$$l < \frac{\cos(\alpha) + 1}{\sin(\alpha)} r.$$

Hydrophilic particles

The case for hydrophilic particles is more complex than the hydrophobic case due to the fact that the equatorial plane of the particle is buried in the ice and r cannot be measured directly. We point out again that one of the advantages of the approach presented in this paper is indeed the possibility of measuring the height of the particles relative to the interface independently of the lateral dimensions, and thus also obtain directly wetting angles for hydrophilic particles with only one measurement. In this case the measured quantities are l and k.

From geometrical considerations based on Fig. S3 we can write:

$$a + \delta + h = l\, tg(\alpha) \quad \Rightarrow \quad a = l\, tg(\alpha) - \delta - h \qquad \text{(S6)}$$

$$(r + a + \delta) = \frac{r}{\cos(\alpha)} \quad \Rightarrow \quad a = r\left[\frac{1}{\cos[(\alpha) - 1]} - \delta\right] \qquad \text{(S7)}$$

By merging (S6) and (S7) we obtain

$$r = \frac{l\,sin(\alpha) - h\cos(\alpha)}{1 - \cos(\alpha)}. \qquad \text{(S8)}$$

The Pythagorean Theorem applied to the triangle defined by the cross section of the particle at the interface and the particle center yields

$$(l-k)^2 + (r-h)^2 = r^2 \qquad \text{(S9)}$$

substituting (S8) into (S9) we get the following equation in h

$$(l-k)^2[1-\cos(\alpha)]^2 + [l\sin(\alpha) - h]^2 = [l\sin(\alpha) - h\cos(\alpha)]^2 \qquad \text{(S10)}$$

solving (S10) we obtain

$$h = \frac{\sin(\alpha)}{1+\cos(\alpha)}\left(l \pm k\sqrt{2l/k - 1}\right). \qquad \text{(S11)}$$

Of the two possible solutions, only the one which fulfils the condition $h = r$ for $\theta=\pi/2$ is valid and therefore we obtain

$$h = \frac{\sin(\alpha)}{1+\cos(\alpha)}\left(l + k\sqrt{2l/k - 1}\right). \qquad \text{(S12)}$$

From Fig. S8 we see that $\theta = \pi/2 - \beta$, and

$$\beta = \arcsin(\Delta/r) = \arcsin\left(\frac{r-h}{r}\right) = \arcsin\left(1 - \frac{h}{r}\right), \qquad \text{(S13)}$$

so, finally, by substituting (S8) and (S12) into (S13) the expression for the contact angle is:

$$\theta = \pi/2 - \sin^{-1}\left[\frac{l\cos(\alpha) - k\sqrt{2l/k - 1}}{l - k\cos(\alpha)\sqrt{2l/k - 1}}\right] = \pi/2 - \sin^{-1}\left[\frac{\frac{l}{k}\cos(\alpha) - \sqrt{2l/k - 1}}{\frac{l}{k} - \cos(\alpha)\sqrt{2l/k - 1}}\right]. \qquad \text{(S14)}$$

We observe that also in this case the contact angle depends only on the ratio l/k. The upper limit for l is determined by the condition of neutral wettability $l = r/\sin(\alpha) = k/[1-\sin(\alpha)]$, while the lower limit is fixed by the geometric fact that the minimum contact angle measurable with the method is $\theta=\alpha$, for which $l=r\cos(\alpha)$ and $k=0$

Supplementary Note 2

Accuracy and resolution of the method

In the following we derive the full expressions for the θ error estimation as reported in the text.

Hydrophobic particles:

From eq. (S5) we observe that $\theta = \theta\left(\frac{l}{r}\right)$, therefore the error in θ is

$$\sigma_\theta = \frac{d\theta}{d\left(\frac{l}{r}\right)}\sigma_{\left(\frac{l}{r}\right)} \quad . \qquad \text{(S15)}$$

By differentiating eq. (S5) we obtain

$$\frac{d\theta}{d\left(\frac{l}{r}\right)} = \frac{\tan(\alpha)}{\sqrt{1-\left(\frac{\tan(\alpha)\,l}{r}-\frac{1}{\cos(\alpha)}\right)^2}} \quad . \qquad \text{(S16)}$$

Given that $\left(\frac{\sigma_{\left(\frac{l}{r}\right)}}{\left(\frac{l}{r}\right)}\right)^2 = \left(\frac{\sigma_l}{l}\right)^2 + \left(\frac{\sigma_r}{r}\right)^2$, we finally get the expression for the error in θ:

$$\sigma_\theta = \sqrt{\frac{1}{1-\left(\tan(\alpha)\frac{l}{r}-\frac{1}{\cos(\alpha)}\right)^2}\left(\frac{\tan(\alpha)}{r}\right)^2\left(\sigma_l^2+\sigma_r^2\left(\frac{l}{r}\right)^2\right)} \quad . \qquad \text{(S17)}$$

Hydrophilic particles:

From eq. (S14) we observe that $\theta = \theta\left(\frac{l}{k}\right)$, therefore the error in θ is

$$\sigma_\theta = \frac{d\theta}{d\left(\frac{l}{k}\right)}\sigma_{\left(\frac{l}{k}\right)} \quad . \qquad \text{(S18)}$$

By differentiating eq. (S14) we obtain

$$\frac{d\theta}{d\left(\frac{l}{k}\right)} = \frac{1}{\sqrt{1-\left(\frac{\frac{l}{k}\cos(\alpha)-\sqrt{\frac{2l}{k}-1}}{\frac{l}{k}-\cos(\alpha)\sqrt{\frac{2l}{k}-1}}\right)^2}} \frac{\left(\frac{l}{k}-1\right)(\sin(\alpha))^2}{\sqrt{\frac{2l}{k}-1}} \frac{1}{\left(\frac{l}{k}-\cos(\alpha)\sqrt{\frac{2l}{k}-1}\right)^2} \tag{S19}$$

Given that $\left(\frac{\sigma_{\left(\frac{l}{k}\right)}}{\left(\frac{l}{k}\right)}\right)^2 = \left(\frac{\sigma_l}{l}\right)^2 + \left(\frac{\sigma_k}{k}\right)^2$, we finally get the expression for the error in θ:

$$\sigma_\theta = \frac{1}{\sqrt{1-\left(\frac{\frac{l}{k}\cos(\alpha)-\sqrt{\frac{2l}{k}-1}}{\frac{l}{k}-\cos(\alpha)\sqrt{\frac{2l}{k}-1}}\right)^2}} \frac{\left(\frac{l}{k}-1\right)(\sin(\alpha))^2}{\sqrt{\frac{2l}{k}-1}} \frac{1}{\left(\frac{l}{k}-\cos(\alpha)\sqrt{\frac{2l}{k}-1}\right)^2} \frac{l}{k}\sqrt{\left(\frac{\sigma_l^2}{l^2}+\frac{\sigma_k^2}{k^2}\right)},$$

which can be further simplified into

$$\sigma_\theta = \frac{\sin(\alpha)}{\sqrt{\frac{2l}{k}-1}} \frac{1}{\left(\frac{l}{k}-\cos(\alpha)\sqrt{\frac{2l}{k}-1}\right)} \frac{1}{k}\sqrt{\left(\sigma_l^2+\sigma_k^2\frac{l^2}{k^2}\right)}. \tag{S20}$$

In both cases the relative errors in measuring *l*, *r* and *k* determine the final accuracy in measuring the contact angles. The limiting factor in measuring accurately the particle dimensions and the shadow length in the SEM images is the pixel size relative to the object size. From sharp SEM images we can measure features with ±1 pixel accuracy (σ_l and σ_k = 1 pixel, σ_r = 0.5 pixel). This means that, regardless of the magnification used, particles with a diameter and a shadow length smaller than 3 pixels were discarded as being not resolvable. As already discussed in the main text, by lowering the shadowing angle we reduce the relative errors in measuring the features in the images and thus we increase accuracy.

From eq. (S17) we also notice that σ_θ diverges approaching the upper limit of $\theta=\pi$ and from plotting the results of eq. (S20) we also see that the errors increase when approaching the lower limit $\theta=\alpha$. This is due to the $\sin^{-1}$ dependence of θ on the measured quantities.

Finally we report that the best resolution previously obtained from raw images after freeze-fracturing and metal coating[41-42] is in the range of 1.5-2 nm laterally[43] and of about 4 nm for a height measurement[44, 45]; statistical image treatments have shown the potential to increase the resolution down to 0.7 nm [46]. The highest resolution we achieved in our SEM images after averaging each image line over at least 10 images was of 0.7 nm/pixel. The spatial resolution of the imaging technique could be pushed even further by fabricating carbon replicas of the frozen interfaces after the cryo-SEM investigation and imaging the replicas with TEM at high resolution.

Supplementary Note 3

Evaluation of AFM-GTT data

The quantities measurable from AFM-GTT experiments are the height *h* and the radius *r'* of the cross-section of each particle protruding from the PDMS surface. Given that the particles are sufficiently large so that tip convolution effects are negligible relative to the particle size, by measuring directly *h* and *r'* and using geometrical arguments, we can define the contact angle θ as:

$$\theta = \sin^{-1}\left(\frac{r'}{r}\right) = \sin^{-1}\left(\frac{r'}{\sqrt{r'^2 + \left(\frac{r'^2 - h^2}{2h}\right)^2}}\right) = \sin^{-1}\left(\frac{2\left(h/r'\right)}{\left(h/r'\right)^2 + 1}\right), \qquad \text{(S23)}$$

where *r* is the actual particle radius. The formula above is valid for hydrophobic particles, like the ones measured in the main paper, for which the equator is buried into the PDMS.

Given that $\left(\frac{\sigma_{\left(\frac{h}{r'}\right)}}{\left(\frac{h}{r'}\right)}\right)^2 = \left(\frac{\sigma_h}{h}\right)^2 + \left(\frac{\sigma_r'}{r'}\right)^2$ and that for AFM images $\sigma_h \ll \sigma_r'$, following the same arguments as in eq. (S15), we obtain

$$\sigma_\theta = \frac{2}{\left(h/r'\right)^2 + 1}\frac{h}{r'^2}\sigma_r', \qquad \text{(S24)}$$

where $\frac{2}{\left(h/r'\right)^2 + 1}$ is $\frac{d\theta}{d\left(\frac{h}{r'}\right)}$.

Equation (S24) has been used in the main text to evaluate the errors for the AFM-GTT data reported in Figure 7.

Supplementary Note 4

Measuring line tension

Using the expression proposed by Aveyard and Clint[15] we define the line tension τ as

$$\tau = \gamma_0 r \sin\theta \left(1 - {}^{\cos\theta_0}/_{\cos\theta}\right) \qquad \text{(S21)}$$

where γ_0 is the interfacial tension between the two fluid phases, θ is the contact angle of a particle with radius *r* and θ_0 is the macroscopic contact angle between the bulk particle material and the two fluid phases. For the data presented in the main text, we chose the macroscopic contact angle as the value of the average contact angle of the 500nm and 200nm amidine latex particles (103°); the choice is justified since this value does not depend on particle size.

From eq. (21) we observe that $\tau = \tau(\theta, r)$, therefore the error in τ is

$$\left(\frac{\sigma_\tau}{\tau}\right)^2 = \left(\frac{\partial\tau}{\partial\theta}\frac{\sigma_\theta}{\theta}\right)^2 + \left(\frac{\partial\tau}{\partial r}\frac{\sigma_r}{r}\right)^2.$$

From which we obtain

$$\sigma_\tau = \tau\sqrt{\left[\left(\gamma_0 r\cos\theta - \frac{\gamma_0 r\cos\theta_0}{\cos^2\theta}\right)^2\left(\frac{\sigma_\theta}{\theta}\right)^2 + \left(\gamma_0 r\sin\theta\left[1 - \frac{\cos\theta_0}{\cos\theta}\right]\right)^2\left(\frac{\sigma_r}{r}\right)^2\right]}, \qquad \text{(S22)}$$

which is used to calculate the y-error bars in Figure 6b.

Supplementary References

41. R. Wepf, T. Richter, M. Sattler, A. Kaech, *Microsc. Microanal.* **10**, 970 (2004).
42. T. Richter *et al.*, *J. Micros.-Oxford* **225**, 201 (2007).
43. O. Kubler, H. Gross, H. Moor, *Ultramicroscopy* **3**, 161 (1978).
44. H. Gross, E. Bas, H. Moor, *J. Cell Bio.* **76**, 712 (1978).
45. H. Gross, O. Kuebler, E. Bas, H. Moor, *J. Cell Biol.* **79**, 646 (1978).
46. S. Scheuring *et al.*, *J. Mol. Biol.* **299**, 1271 (2000).